Journal of Applied Fluid Mechanics, Vol. 15, No. 3, pp. 815-829, 2022.
Available online at www.jafmonline.net, ISSN 1735-3572, EISSN 1735-3645.
https://doi.org/10.47176/jafm.15.03.33193

A General Approach for Flow Optimization and Drag Reduction in Turbulent Pipe Flows

J. Guo[1], K. Luo[†1,2], Z. He[1], S. Wu[1] and J. Fan[1,2]

[1.] *State Key Laboratory of Clean Energy Utilization, Zhejiang University, Hangzhou, Zhejiang, 310027, China*
[2.] *Shanghai Institute for Advanced Study of Zhejiang University,Shanghai 200120,China*

†*Corresponding Author Email: zjulk@zju.edu.cn*

(Received July 13, 2021; accepted January 4, 2022)

ABSTRACT

Flow optimization and drag reduction are of great importance in industrial applications. However, most of the structural optimization and drag reduction in pipe flows are based on industrial experience or a large number of experiments, and there is a lack of general theoretical guidance. In the present work, a general approach for flow optimization and drag reduction in turbulent pipe flows is developed based on the irreversibility of flow process and the principle of minimum mechanical energy dissipation. Considering that the effective viscosity coefficient is related to the space coordinates, the field synergy equation of turbulent flow is derived. The reliability and performance of the field synergy principle of turbulent flow as well as the general approach are then evaluated and validated in a turbulent parallel flow conduit, and finally applied to industrial pipe flows. It demonstrates that the present approach is able to optimize flow field for different purposes by adding speed splitter or deflector as an interface at proper locations to alter the interactions between fluid and wall. It is robust and easy to implement, which provides general theoretical guidance for flow optimization and drag reduction in turbulent pipe flows.

Keywords: Field Synergy Principle; Minimum mechanical energy dissipation principle; Effective viscosity coefficient; Pipe flow; Drag reduction; Flow optimization.

1. INTRODUCTION

Pipeline network is very common in industries, in which fluids are transported from one location to another. However, due to unreasonable design of pipeline and the viscous dissipation characteristics of the fluid, the energy waste cannot be avoided. Therefore, it is of great importance to optimize fluid flow in the pipeline.

Recently, computational fluid dynamics (CFD) has been utilized to study the flow field optimization in tube pipeline. By analyzing the results of the velocity stream distribution and pressure distribution obtained from CFD, the design of the internal structure of the tube is improved and the flow field is optimized (Marjavaara and Lundström 2006). Jia *et al.* (2011) used the RNG k-ε model to simulate the flow field in the elbow pipes, and found that installing deflectors at certain locations inside the elbow can significantly reduce the generation of vortices and improve the distributions of both speed and pressure in the fluid. Khanorkar and Thombre (2013) studied natural convection flow of water through vertical pipe, and analyzed the effect of the physical parameters such as diameter, length, and heat flux on the outlet flow parameters. Many other researchers had used CFD methods to simulate the flow fields in different pipes, analyzed the flow resistance and proposed corresponding improvement solutions (Addy *et al.* 1985; Yue 2011; Hu *et al.* 2012; Yang *et al.* 2013; Kim *et al.* 2014; Zhao *et al.* 2015; Wu 2013; Hui 2014; Rao *et al.* 2016; Dutta *et al.* 2016; Rao 2018; Okafor *et al.* 2020).

However, the optimization of pipelines in the above-mentioned studies has lacked a unified and reliable theoretical basis. Guo *et al.* (1998) proposed field synergy principle (FSP), which indicates that the heat transfer performance depends not only on the velocity field and the temperature field, but also on their synergy. Tao *et al.* (2019) pointed out that the heat-line visualized the heat transfer path and studied the heat transfer mechanism with FSP. Considering the similarity between momentum transfer and heat transfer, Chen *et al.* (2007) proposed the principle of minimum mechanical energy dissipation. Combined with this principle, Chen *et al.* (2008) proposed the FSP of fluid flow which is suitable for steady-state, incompressible laminar flow. They reasoned that the lower the degree of synergy between the velocity and velocity gradient, the smaller the mechanical energy

dissipation and the lower the flow resistance. On this basis, Zuo (2012) and Lv (2014) further derived a collaborative mathematical model for compressible laminar flow, and successfully applied the model to reduce the drag of flow field. Lu *et al*. (2014) further collated and deduced the equations, and established an incompressible turbulence field synergy model. The model was validated and the concept of fully coordinated flow field was proposed for flow optimization. Zhang *et al*. (2014) presented the compressible fluid flow field synergy principle, which presented as an effective theoretical guide to reduce the drag during compressible flow.

However, the above studies did not consider the effect of the effective viscous coefficient in the field synergy model. This work rederives the turbulent field synergy principle by volume integration of the governing equations of turbulent flow based on the irreversibility of flow process and the principle of minimum mechanical energy dissipation. It is demonstrated that the flow resistance is not only related to the field synergy number, but also related to the effective viscosity coefficient. A general approach for flow optimization and drag reduction in turbulent pipe flows is then developed and validated in a turbulent parallel flow conduit, and finally applied to industrial pipe flows.

2. MATHEMATICAL MODELS

2.1 Turbulence field synergy principle

Applying the field synergy principle to turbulent flow, the momentum equation of the incompressible turbulent flow with steady state and without volume force can be obtained as follows (Tao 2001):

$$\rho u_j \frac{\partial u_i}{\partial x_j} = -\frac{\partial P}{\partial x_i} + \frac{\partial}{\partial x_j}\left[\mu_{eff}\left(\frac{\partial u_i}{\partial x_j} + \frac{\partial u_j}{\partial x_i}\right) - \frac{2}{3}\rho k \delta_{ij}\right] \tag{1}$$

Where ρ is the density of the fluid medium, P is the pressure, u_i, u_j is the component of the velocity vector in the i, j direction respectively, k is the kinetic energy coefficient; δ_{ij} is the unit second order tensor; μ_{eff} is the effective viscosity coefficient including laminar viscosity coefficient μ and the turbulent viscosity coefficient μ_t.

Integrate Eq. (1) over the entire flow area Ω, one has:

$$\int_\Omega \rho u_j \frac{\partial u_i}{\partial x_j} dV = -\int_\Omega \frac{\partial p}{\partial x_i} dV + \int_\Omega \frac{\partial}{\partial x_j}\left[\mu_{eff}\left(\frac{\partial u_i}{\partial x_j} + \frac{\partial u_j}{\partial x_i}\right) - \frac{2}{3}\rho k \delta_{ij}\right] dV \tag{2}$$

Where V is the volume of the flow field. The second item on the right side of Eq. (2) can be split into:

$$\int_\Omega \frac{\partial}{\partial x_j}\left[\mu_{eff}\left(\frac{\partial u_i}{\partial x_j} + \frac{\partial u_j}{\partial x_i}\right) - \frac{2}{3}\rho k \delta_{ij}\right] dV = \int_\Omega \frac{\partial}{\partial x_j}\left(\mu_{eff}\frac{\partial u_i}{\partial x_j} - \frac{2}{3}\rho k \delta_{ij}\right) dV + \int_\Omega \frac{\partial}{\partial x_j}\left(\mu_{eff}\frac{\partial u_j}{\partial x_i}\right) dV \tag{3}$$

The first term of Eq. (3) can be converted to an area integral by Green's formula:

$$\int_\Omega \frac{\partial}{\partial x_j}\left(\mu_{eff}\frac{\partial u_i}{\partial x_j} - \frac{2}{3}\rho k \delta_{ij}\right) dV = \int_\Gamma \left(\mu_{eff}\frac{\partial u_i}{\partial x_j} - \frac{2}{3}\rho k \delta_{ij}\right)\cdot \mathbf{n} dS \tag{4}$$

Where Γ is the outer boundary of the flow area, S is the outside surface area of the boundary, $\mathbf{n}$ is the outward unit normal vector of the outer boundary.

For the incompressible fluid, $\frac{\partial}{\partial x_j}\left(\frac{\partial u_j}{\partial x_i}\right) = \frac{\partial}{\partial x_i}\left(\frac{\partial u_j}{\partial x_j}\right) = 0$, then the second term on the right side of Eq. (3) could be converted to:

$$\int_\Omega \frac{\partial}{\partial x_j}\left(\mu_{eff}\frac{\partial u_j}{\partial x_i}\right) dV = \int_\Omega \frac{\partial \mu_{eff}}{\partial x_j}\frac{\partial u_j}{\partial x_i} dV + \int_\Omega \mu_{eff}\frac{\partial}{\partial x_j}\left(\frac{\partial u_j}{\partial x_i}\right) dV = \int_\Omega \frac{\partial \mu_{eff}}{\partial x_j}\frac{\partial u_j}{\partial x_i} dV \tag{5}$$

Substitute Eq. (4) and Eq. (5) into Eq. (2):

$$\int_\Omega \rho u_j \frac{\partial u_i}{\partial x_j} dV = -\int_\Omega \frac{\partial p}{\partial x_i} dV + \int_\Gamma \left(\mu_{eff}\frac{\partial u_i}{\partial x_j} - \frac{2}{3}\rho k \delta_{ij}\right)\cdot \mathbf{n} dS + \int_\Omega \frac{\partial \mu_{eff}}{\partial x_j}\frac{\partial u_j}{\partial x_i} dV \tag{6}$$

$D = \frac{V}{S}$ is defined as the characteristic length and the following dimensionless variables can be introduced (represented by the superscript "—"):

$$\overline{u_i} = u_i / u_{in}, \overline{u_j} = u_j / u_{in}, \quad \nabla \overline{u_i} = \frac{\nabla u_i}{u_{in}/D}, d\overline{V} = \frac{dV}{V}, d\overline{S} = \frac{dS}{S} \tag{7}$$

Then Eq. (6) could be converted to (Chen *et al*. 2008):

$$-\frac{D}{\rho u_{in}^2}\int_\Omega \frac{\partial P}{\partial x_i} d\overline{V} = -\frac{1}{\rho u_{in} D}\int_\Gamma \left(\mu_{eff}\nabla \overline{u_i} - \frac{2D}{3u_{in}}\rho k \delta_{ij}\right)\cdot \mathbf{n} d\overline{S} + \int_\Omega \overline{U}\cdot \nabla \overline{u_i} d\overline{V} - \frac{D}{\rho u_{in}}\int_\Omega \frac{\partial \mu_{eff}}{\partial x_j}\frac{\partial \overline{u_j}}{\partial x_i} dV \tag{8}$$

$\overline{U}$ is the dimensionless velocity vector. V is the volume of the flow field, $d\overline{V}$ is the dimensionless variable introduced by Eq. (7).

The left side of Eq. (8) is defined as the dimensionless pressure gradient DC_i:

$$DC_i = -\frac{D}{\rho u_{in}^2}\int_\Omega \frac{\partial p}{\partial x_i}d\overline{V} \tag{9}$$

Equation (9) shows that the dimensionless pressure gradient is related to the inlet parameters of the flow field and is inversely proportional to the kinetic energy at the inlet in the direction opposite to that of the pressure change.

The second term on the right side of Eq. (8) is the integral of the dot product between the dimensionless velocity vector and the dimensionless velocity gradient over the entire flow region:

$$FS_m = \int_\Omega \overline{U}\cdot\nabla\overline{u_i}d\overline{V} = \int_\Omega \left|\overline{U}\right|\left|\nabla\overline{u_i}\right|\cos\beta_m d\overline{V} \tag{10}$$

Where β_m is the angle between the velocity vector and the velocity gradient vector which is between 0-π/2, FS_m is the turbulence field synergy number, which indicates the degree of synergy between the velocity field and the velocity gradient field. The value of FS_m is related to β_m. The bigger β_m ,the smaller $\cos\beta_m$, the smaller FS_m.

Equation (8) demonstrates the field synergy principle of turbulent flow. The dimensionless pressure gradient characterizes the change in pressure drop during fluid flow, i.e., the magnitude of the flow resistance. As seen in Eq. (8), when the inlet flow rate or inlet velocity is given, the lower the field synergy, i.e., the smaller the field synergy number, the smaller the dimensionless pressure gradient, and the smaller the resistance of the fluid (Chen *et al.* 2008).

In addition, Eq. (8) can also explain that the dimensionless pressure gradient is also related to $\int_\Omega \frac{\partial \mu_{eff}}{\partial x_j}\frac{\partial \overline{u_j}}{\partial x_i}dV$, and the larger the $\int_\Omega \frac{\partial \mu_{eff}}{\partial x_j}\frac{\partial \overline{u_j}}{\partial x_i}dV$, the smaller the flow resistance. From the perspective of mechanical energy dissipation, the relationship between the effective viscosity coefficient and the flow resistance will be discussed in the next section.

2.2 Minimum mechanical energy dissipation

Flow resistance is the reaction force caused by the fluid viscosity that hinders the flow, and leads to the mechanical energy dissipation of the fluid. Fluid flow is an irreversible process. The amount of mechanical energy dissipation reflects the degree of irreversibility of fluid flow.

When the mechanical energy dissipation is minimal, the flow resistance of the flow field is minimum. The flow field with the least resistance can be obtained by minimizing the dissipation function under given constraints. This is the principle of minimum mechanical energy dissipation.

$$\tau = -\mu\, du_i/dx_j \tag{11}$$

Equation (11) reflects the relationship between the shearing stress and the rate of shearing strain of Newtonian fluid, or the relationship between momentum transport and velocity gradient. μ is the viscosity, which is an important physical parameter of the liquid.

Due to the velocity gradient caused by the deformation of the fluid flow, momentum diffuses within the fluid. According to the energy conservation equation, the mechanical energy dissipation of the fluid can be expressed as (Rodriguez 2019; Chen *et al.* 2008):

$$\Phi = \mu_{eff}\left[\begin{array}{l} 2(\frac{\partial u}{\partial x})^2+2(\frac{\partial v}{\partial y})^2+2(\frac{\partial w}{\partial z})^2 \\ +(\frac{\partial u}{\partial x}+\frac{\partial v}{\partial y})^2+(\frac{\partial u}{\partial z}+\frac{\partial w}{\partial x})^2+(\frac{\partial v}{\partial z}+\frac{\partial w}{\partial y})^2 \end{array}\right] \tag{12}$$

Where μ_{eff} is the effective viscosity coefficient of the fluid, $\mu_{eff} = \mu + \mu_t$, and μ_t is the turbulent viscosity, or eddy viscosity, which is a function of spatial coordinates and depends on the flow state, not a physical parameter. It's an improvement compared with the study of Lv (2014). λ is the thermal conductivity of the fluid. $\boldsymbol{U}$ is the velocity field.

2.3 Turbulence Field synergy equations

In order to reduce the flow resistance as much as possible, the total amount of mechanical energy dissipation in the whole flow field is minimized, which is the goal of flow field optimization.

According to the principle of minimum mechanical energy dissipation, the equation satisfied by the optimal velocity field can be obtained by the variation principle. Its optimization model can include optimized objects, optimization goals, constraints, and boundary conditions.

1. The optimization object: the velocity field $\boldsymbol{U}$.
2. The optimization goal is to take the extreme value of the total amount of mechanical energy dissipation in the entire basin, which can be expressed as:

$$\delta\int_\Omega \Phi dV = 0 \tag{13}$$

3. Constraint condition is mass conservation:

$$\nabla\cdot(\rho\boldsymbol{U}) = 0 \tag{14}$$

4. The velocity boundary condition is a constant boundary speed, which is described by a variation symbol:

$$\delta\boldsymbol{U}\big|_{in} = 0 \tag{15}$$

The process of solving the optimal velocity field is to find the function solution satisfying the above optimization model in the function space of the velocity vector field $\boldsymbol{U}$, which belongs to the variational problem. First of all, the Lagrangian function by variational method is constructed:

$$J = \int_\Omega \left[\Phi + \lambda\nabla\cdot\boldsymbol{U}\right]dV \tag{16}$$

Where λ is the Lagrange multiplier, which is a function of $\boldsymbol{U}$ and spatial position. Then, taking the variation for velocity u to get:

$$\delta J_u = \int_\Omega \left[\delta\Phi + \lambda \frac{\partial}{\partial x}(\delta u) \right] dV = \int_\Omega \left\{ \begin{array}{l} \dfrac{\Phi}{\mu_{eff}} \delta\mu_{eff} \\ +\mu_{eff}\delta \left[\begin{array}{l} 2(\dfrac{\partial u}{\partial x})^2 \\ +(\dfrac{\partial u}{\partial y}+\dfrac{\partial v}{\partial x})^2 \\ +(\dfrac{\partial u}{\partial z}+\dfrac{\partial w}{\partial x})^2 \end{array} \right] \\ +\lambda \dfrac{\partial}{\partial x}(\delta u) \end{array} \right\} dV = 0 \tag{17}$$

Equation (17) can be transformed as follows:

$$\int_\Omega \left\{ \begin{array}{l} \dfrac{\Phi}{\mu_{eff}} \dfrac{\partial \mu_{eff}}{\partial u} \delta u \\ +2\nabla\cdot\left(\mu_{eff}\nabla u \delta u\right) \\ -2\left[\nabla\cdot\left(\mu_{eff}\nabla u\right)\right]\delta u \\ +2 \left[\begin{array}{l} \dfrac{\partial}{\partial x}\left(\partial\mu_{eff}\delta u\right)\dfrac{\partial u}{\partial x} \\ +\dfrac{\partial}{\partial y}\left(\partial\mu_{eff}\delta u\right)\dfrac{\partial v}{\partial x} \\ +\dfrac{\partial}{\partial z}\left(\partial\mu_{eff}\delta u\right)\dfrac{\partial w}{\partial x} \end{array} \right] \\ -2 \left(\begin{array}{l} \dfrac{\partial\mu_{eff}}{\partial x}\dfrac{\partial u}{\partial x}+\dfrac{\partial\mu_{eff}}{\partial y}\dfrac{\partial v}{\partial x} \\ +\dfrac{\partial\mu_{eff}}{\partial z}\dfrac{\partial w}{\partial x} \end{array} \right) \delta u \\ +\dfrac{\partial}{\partial x}(\lambda\delta u) - \dfrac{\partial\lambda}{\partial x}\delta u \end{array} \right\} dV = 0 \tag{18}$$

Combining similar terms leads to:

$$\begin{array}{l} \displaystyle\int_\Omega \left\{ \begin{array}{l} 2\nabla\cdot\left(\mu_{eff}\nabla u\delta u\right)+ \\ 2\left[\begin{array}{l} \dfrac{\partial}{\partial x}\left(\partial\mu_{eff}\delta u\right)\dfrac{\partial u}{\partial x} \\ +\dfrac{\partial}{\partial y}\left(\partial\mu_{eff}\delta u\right)\dfrac{\partial v}{\partial x} \\ +\dfrac{\partial}{\partial z}\left(\partial\mu_{eff}\delta u\right)\dfrac{\partial w}{\partial x} \end{array} \right] \\ +\dfrac{\partial}{\partial x}\left(\lambda\delta u\right) \end{array} \right\} dV \\ +\displaystyle\int_\Omega \left\{ \begin{array}{l} \dfrac{\Phi}{\mu_{eff}}\dfrac{\partial\mu_{eff}}{\partial u} - 2\left[\nabla\cdot\left(\mu_{eff}\nabla u\right)\right] \\ -2\left(\begin{array}{l} \dfrac{\partial\mu_{eff}}{\partial x}\dfrac{\partial u}{\partial x}+\dfrac{\partial\mu_{eff}}{\partial y}\dfrac{\partial v}{\partial x} \\ +\dfrac{\partial\mu_{eff}}{\partial z}\dfrac{\partial w}{\partial x} \end{array} \right) \\ -\dfrac{\partial\lambda}{\partial x} \end{array} \right\} \delta u dV = 0 \end{array} \tag{19}$$

The left terms in Eq. (19) are transformed by the Green's formula as follows:

$$\int_\Omega \left[2\nabla\cdot\left(\mu_{eff}\nabla u\delta u\right) \right] dV = \int_\Gamma \left(2\mu_{eff}\nabla u\delta u\right)\cdot dS \tag{20}$$

$$\int_\Omega \frac{\partial}{\partial x}(\lambda\delta u) dV = \int_\Gamma \lambda\delta U \cdot dS \tag{21}$$

$$\begin{array}{l} \displaystyle\int_\Omega 2 \left[\begin{array}{l} \dfrac{\partial}{\partial x}\left(\partial\mu_{eff}\delta u\right)\dfrac{\partial u}{\partial x}+\dfrac{\partial}{\partial y}\left(\partial\mu_{eff}\delta u\right)\dfrac{\partial v}{\partial x} \\ +\dfrac{\partial}{\partial z}\left(\partial\mu_{eff}\delta u\right)\dfrac{\partial w}{\partial x} \end{array} \right] \\ = \displaystyle\int_\Omega 2 \left[\begin{array}{l} \dfrac{\partial\left(\partial\mu_{eff}\delta u\dfrac{\partial u}{\partial x}\right)}{\partial x} \\ +\dfrac{\partial\left(\partial\mu_{eff}\delta u\dfrac{\partial v}{\partial x}\right)}{\partial y} \\ +\dfrac{\partial\left(\partial\mu_{eff}\delta u\dfrac{\partial w}{\partial x}\right)}{\partial z} \end{array} \right] dV \\ -\displaystyle\int_\Omega 2\mu_{eff}\left(\frac{\partial^2 u}{\partial x^2}+\frac{\partial^2 v}{\partial x\partial y}+\frac{\partial^2 w}{\partial x\partial z}\right)\delta u dV \\ = \displaystyle\int_\Gamma 2\mu_{eff}\delta u\left(\frac{\partial u}{\partial x},\frac{\partial v}{\partial x},\frac{\partial w}{\partial x}\right)\cdot dS \\ -\displaystyle\int_\Omega 2\mu_{eff}\left(\frac{\partial^2 u}{\partial x^2}+\frac{\partial^2 v}{\partial x\partial y}+\frac{\partial^2 w}{\partial x\partial z}\right)\delta u dV \end{array} \tag{22}$$

Equations (20)-(22) are substituted into Eq. (19):

$$\begin{array}{l} \displaystyle\int_\Gamma \left[\begin{array}{l} 2\mu_{eff}\nabla u\delta u+\lambda\delta\boldsymbol{U} \\ +2\mu_{eff}\delta u\left(\dfrac{\partial u}{\partial x},\dfrac{\partial v}{\partial x},\dfrac{\partial w}{\partial x}\right) \end{array} \right]\cdot dS \\ +\displaystyle\int_\Omega \left\{ \begin{array}{l} \dfrac{\Phi}{\mu_{eff}}\dfrac{\partial\mu_{eff}}{\partial u} \\ -2\left[\nabla\cdot\left(\mu_{eff}\nabla u\right)\right]-\dfrac{\partial\lambda}{\partial x} \\ -2\left(\begin{array}{l} \dfrac{\partial\mu_{eff}}{\partial x}\dfrac{\partial u}{\partial x} \\ +\dfrac{\partial\mu_{eff}}{\partial y}\dfrac{\partial v}{\partial x} \\ +\dfrac{\partial\mu_{eff}}{\partial z}\dfrac{\partial w}{\partial x} \end{array} \right) \\ -2\mu_{eff}\left(\begin{array}{l} \dfrac{\partial^2 u}{\partial x^2}+\dfrac{\partial^2 v}{\partial x\partial y} \\ +\dfrac{\partial^2 w}{\partial x\partial z} \end{array} \right) \end{array} \right\} \delta u dV = 0 \end{array} \tag{23}$$

Because of the arbitrariness of $\delta \boldsymbol{U}$, the governing equations and boundary conditions are:

$$\begin{aligned}&\nabla\cdot\left(\mu_{eff}\nabla u\right)-\frac{\Phi}{2\mu_{eff}}\frac{\partial\mu_{eff}}{\partial u}+\frac{\partial\mu_{eff}}{\partial x}\frac{\partial u}{\partial x}\\&+\frac{\partial\mu_{eff}}{\partial y}\frac{\partial v}{\partial x}+\frac{\partial\mu_{eff}}{\partial z}\frac{\partial w}{\partial x}\\&+\frac{1}{2}\frac{\partial\lambda}{\partial x}+\mu_{eff}\left(\frac{\partial^2 u}{\partial x^2}+\frac{\partial^2 v}{\partial x\partial y}+\frac{\partial^2 w}{\partial x\partial z}\right)=0\end{aligned} \tag{24}$$

Similarly, take variation for the speed v , w to get:

$$\begin{aligned}&\nabla\cdot\left(\mu_{eff}\nabla v\right)-\frac{\Phi}{2\mu_{eff}}\frac{\partial\mu_{eff}}{\partial v}\\&+\frac{\partial\mu_{eff}}{\partial x}\frac{\partial u}{\partial y}+\frac{\partial\mu_{eff}}{\partial y}\frac{\partial v}{\partial y}+\frac{\partial\mu_{eff}}{\partial z}\frac{\partial w}{\partial y}\\&+\frac{1}{2}\frac{\partial\lambda}{\partial y}+\mu_{eff}\left(\frac{\partial^2 u}{\partial x\partial y}+\frac{\partial^2 v}{\partial y^2}+\frac{\partial^2 w}{\partial y\partial z}\right)=0\end{aligned} \tag{25}$$

$$\begin{aligned}&\nabla\cdot\left(\mu_{eff}\nabla w\right)-\frac{\Phi}{2\mu_{eff}}\frac{\partial\mu_{eff}}{\partial w}\\&+\frac{\partial\mu_{eff}}{\partial x}\frac{\partial u}{\partial z}+\frac{\partial\mu_{eff}}{\partial y}\frac{\partial v}{\partial z}+\frac{\partial\mu_{eff}}{\partial z}\frac{\partial w}{\partial z}\\&+\frac{1}{2}\frac{\partial\lambda}{\partial z}+\mu_{eff}\left(\frac{\partial^2 u}{\partial x\partial z}+\frac{\partial^2 v}{\partial y\partial z}+\frac{\partial^2 w}{\partial z^2}\right)=0\end{aligned} \tag{26}$$

Equations (24)-(26) are the field synergy equations for turbulent flow which form a closed equation group with the continuity equation and the energy conservation equation. With some boundary conditions and constraints, the relevant physical quantities can be solved numerically to get the optimal velocity field with the smallest mechanical energy dissipation.

λ in Eqs. (24)-(26) can be formulated as:

$$\lambda=-2p_{eff}=-2\left(p+2\rho k/3\right) \tag{27}$$

Here p_{eff} is the effective pressure under turbulent flow.

Substituting Eq. (27) into Eqs. (24)-(26), it can be found that they are very similar to momentum equation Eq. (1), yet they have a few more terms than Eq. (1). The extra terms in the x, y, and z directions are expressed as Eqs. (28)-(30):

$$\begin{aligned}F_x=&\rho\left(u\frac{\partial u}{\partial x}+v\frac{\partial u}{\partial y}+w\frac{\partial u}{\partial z}\right)-\frac{\Phi}{2\mu_{eff}}\frac{\partial\mu_{eff}}{\partial u}\\&+\frac{\partial\mu_{eff}}{\partial x}\frac{\partial u}{\partial x}+\frac{\partial\mu_{eff}}{\partial y}\frac{\partial v}{\partial x}+\frac{\partial\mu_{eff}}{\partial z}\frac{\partial w}{\partial x}\\&+\mu_{eff}\left(\frac{\partial^2 u}{\partial x^2}+\frac{\partial^2 v}{\partial x\partial y}+\frac{\partial^2 w}{\partial x\partial z}\right)\end{aligned} \tag{28}$$

$$\begin{aligned}F_y=&\rho\left(u\frac{\partial v}{\partial x}+v\frac{\partial v}{\partial y}+w\frac{\partial v}{\partial z}\right)-\frac{\Phi}{2\mu_{eff}}\frac{\partial\mu_{eff}}{\partial v}\\&+\frac{\partial\mu_{eff}}{\partial x}\frac{\partial u}{\partial y}+\frac{\partial\mu_{eff}}{\partial y}\frac{\partial v}{\partial y}+\frac{\partial\mu_{eff}}{\partial z}\frac{\partial w}{\partial y}\\&+\mu_{eff}\left(\frac{\partial^2 u}{\partial x\partial y}+\frac{\partial^2 v}{\partial y^2}+\frac{\partial^2 w}{\partial y\partial z}\right)\end{aligned} \tag{29}$$

$$\begin{aligned}F_z=&\rho\left(u\frac{\partial w}{\partial x}+v\frac{\partial w}{\partial y}+w\frac{\partial w}{\partial z}\right)-\frac{\Phi}{2\mu_{eff}}\frac{\partial\mu_{eff}}{\partial w}\\&+\frac{\partial\mu_{eff}}{\partial x}\frac{\partial u}{\partial z}+\frac{\partial\mu_{eff}}{\partial y}\frac{\partial v}{\partial z}+\frac{\partial\mu_{eff}}{\partial z}\frac{\partial w}{\partial z}\\&+\mu_{eff}\left(\frac{\partial^2 u}{\partial x\partial z}+\frac{\partial^2 v}{\partial y\partial z}+\frac{\partial^2 w}{\partial z^2}\right)\end{aligned} \tag{30}$$

Equations (28)-(30) are obtained when the ideal flow field is solved according to the principle of minimum mechanical energy dissipation. It is an additional volume force in the original flow field, so this force is called the additional volume force.

By adding the additional volume force as the source term to the momentum equation, an additional velocity is generated in the original velocity field, and an ideal flow field with minimum mechanical energy dissipation and minimum flow resistance can be obtained.

Although the ideal flow field is not possible to obtain in actual applications, it can provide guidance for optimizing the flow field and making the actual flow field as close as possible to the ideal flow field. This is a general approach that can be used for various industrial flow optimizations.

3. NUMERICAL VALIDATION

Before application to practical engineering, it is important to validate the field synergy principle for turbulent flow and evaluate its performance for flow optimization in pipeline. The parallel flow conduit is a relatively simple conduit which includes the process of fluid splitting and confluence as well as the process of changing the direction of fluid flow velocity. It is used as a benchmark case to validate and evaluate the turbulence field synergy principle in this section. The structure of parallel flow conduit is shown in Fig. 1, and the unit of length is mm.

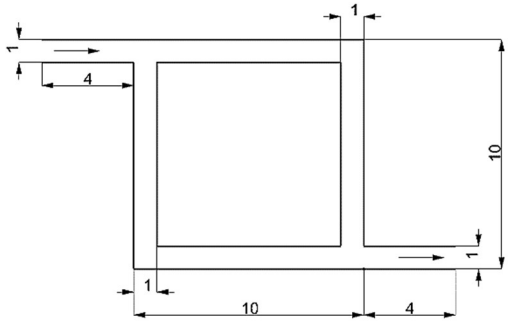

Fig. 1. Structure of parallel flow conduit.

3.1 The original turbulent parallel flow conduit

The turbulent flow of air with an inlet speed of 10 m/s in a parallel flow conduit is simulated using the ANSYS Fluent software. The standard *k-ε* turbulence model is utilized. The pressure and velocity are solved by using the SIMPLE algorithm. The discretization of the original governing equations is conducted by using the second order upwind-differencing scheme. The density of air is 1.225kg/m^3. The dynamic viscosity of air is 1.7894×10^{-5}kg/(m·s).

Figure 2 shows the distribution of pressure, velocity and streamline in the original parallel flow conduit. It is clear there is a vortex in the first bifurcation area where the flow is split. As the initial flow direction is horizontal, most of the fluid flows to the right branch under the influence of inertia, and only a small part flows to the below branch. At the same time, the fluid flowing to the below branch tends to be distributed on the right side, which drives the originally still air on the left side to move downward and form a backflow, that is, a counterclockwise vortex. This non-uniform distribution of the flow results in a high flow velocity near the wall surface and a higher viscous resistance as well higher viscous dissipation in the region of the vortex. As a consequence, the pressure drop across the inlet and outlet of the parallel flow pipe is 163.73pa, and the total amount of mechanical energy consumption is 0.68W.

3.2 The optimized turbulent parallel flow conduit

According to the turbulence field synergy principle, adding the additional volume force as the source term to the momentum equation, the ideal flow field can be obtained, as shown in Fig. 3.

Compared with the pressure field in the original condition, the pressure change is relatively small in the flow process. However, the velocity and streamline distribution becomes quite uniform. The flow along the branches in the horizontal and the vertical directions is roughly the same amount without the vortex. It indicates that the additional volume force counteracts the effect of fluid inertia in the flow field, thereby changes the velocity and streamline distribution so that the mechanical energy dissipation is minimum. As a result, the pressure drop becomes 74.72Pa, which is 54.63% lower than the original flow field. The energy dissipation is 0.48W, which is 29.37% lower than the original flow field.

Inspired by the flow field distribution characteristics under ideal condition, the original flow field can be optimized by adding a speed splitter or a baffle.

The ideal flow field calculated from the field synergy equations can be used as the theoretical guidance basis for adding the speed distributor to optimize the flow field.

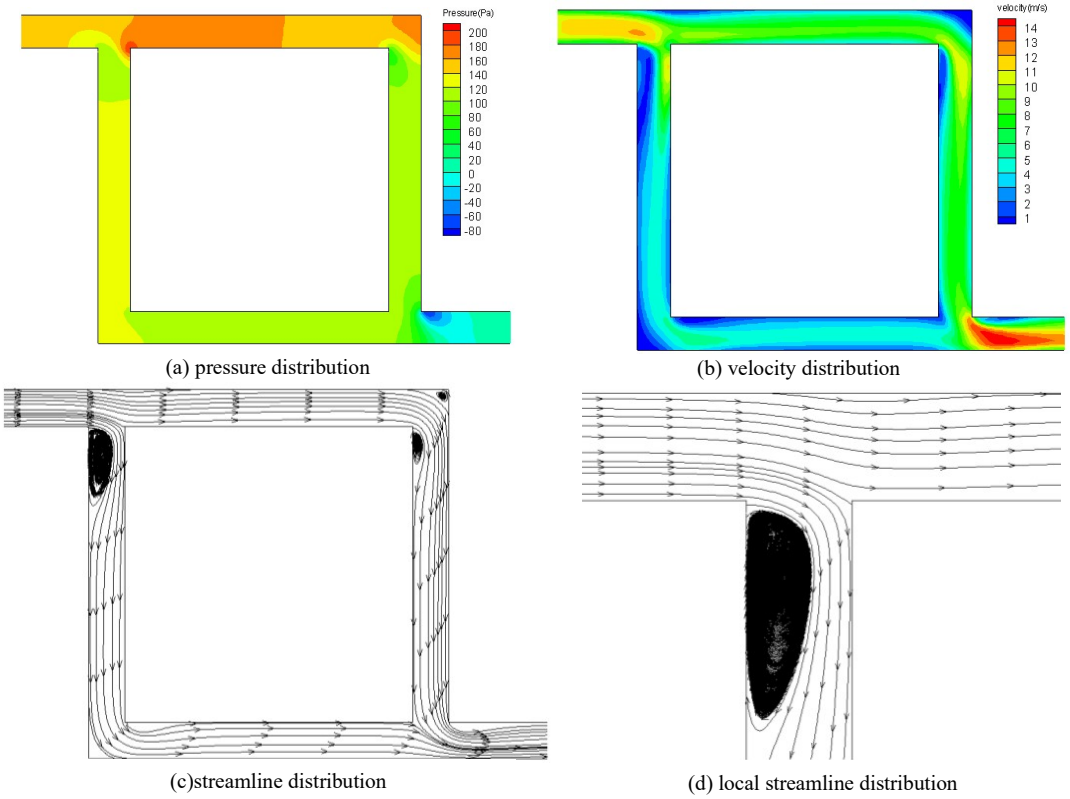

(a) pressure distribution

(b) velocity distribution

(c)streamline distribution

(d) local streamline distribution

Fig. 2. Original parallel flow conduit.

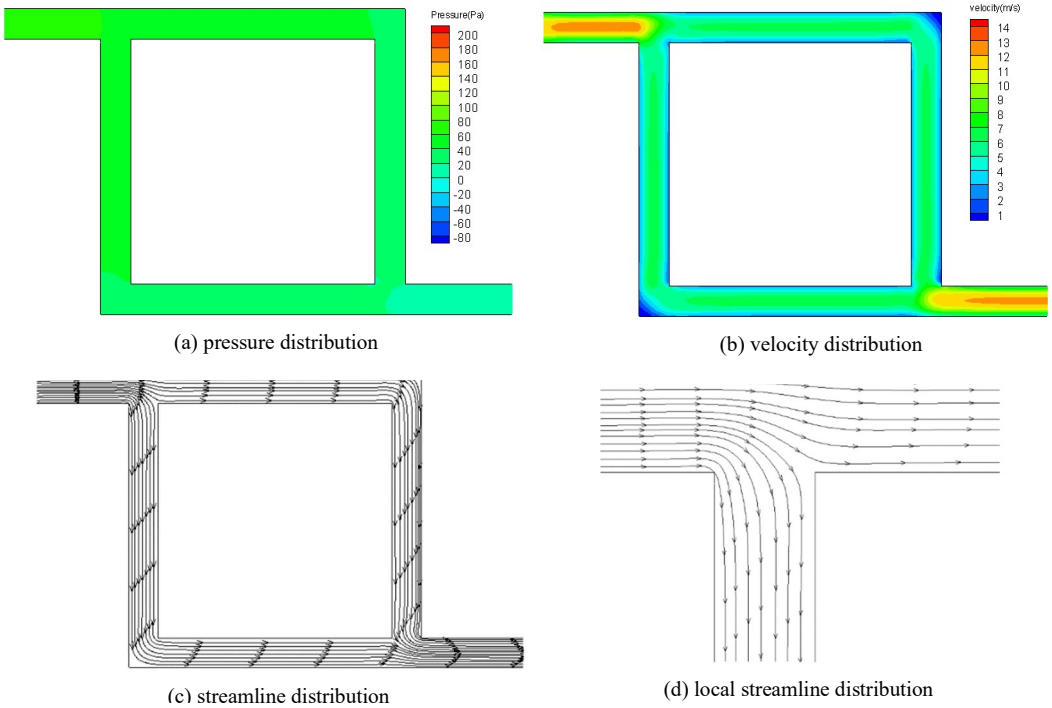

(a) pressure distribution

(b) velocity distribution

(c) streamline distribution

(d) local streamline distribution

Fig. 3. Ideal flow in the parallel conduit.

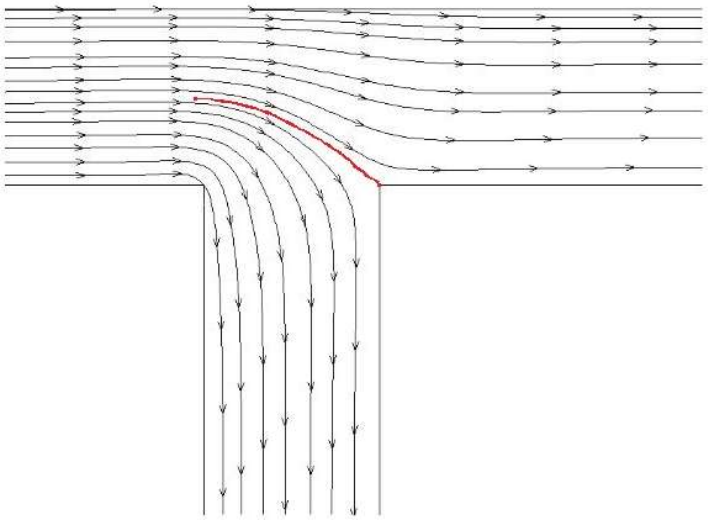

Fig. 4. Principle of designing the baffle.

The starting point should be at the point where the fluid begins to bifurcate. It's easy to understand that the end of the baffle should be at the midpoint of the branch of the pipeline. To make the actual flow field as close to the ideal flow field as possible, the shape of the baffle should be in line of the middle streamline of the conduit, as shown in Fig. 4.

The speed splitter acts as an internal interface and changes the local flow through wall-fluid interaction. Although a vortex is generated, the pressure of the entire flow field is reduced, and the position with the highest flow rate appears in the middle of the pipeline, instead of being distributed near the wall, as shown in Fig. 5. As a result, the pressure drop of the flow field after adding the speed distributor is 149.045pa, which is 8.97% less than that of the original flow field. The total mechanical energy dissipation is 0.64pa, which is 5.88% less than that of the original flow field. Compared with the results under laminar flow conditions (Chen *et al.* 2008), the percentage of the pressure drop and mechanical energy dissipation is larger in the present turbulent flow condition, indicating that it has a more significant effect on drag reduction in turbulence. These results demonstrate that the ideal flow field from the turbulence field synergy equations can serve as a general guide for flow optimization in pipeline.

3.3 Analysis of the field synergy angle

In order to further understand the physical meaning of the field synergy principle and the relationship between the flow field synergy angle and the flow resistance, the cosine value of the field synergy angle in the original flow field is calculated and shown in Fig. 6. In the upper and lower horizontal branches, the cosine value of the synergy angle is very small, indicating that the flow resistance and pressure drop are relatively small. But in the left and right vertical branches, the cosine value of the synergy angle is quite large, which suggests that the flow resistance and pressure drop are relatively large.

The cosine of the field synergy angle in different directions can only reflect the field synergy in a certain direction. In order to comprehensively compare the common effect of the field synergy in the two directions on the entire flow field, the average of the squares of values in the two directions is calculated, and its distribution in the flow field is shown in Fig.7.

It is observed that the cosine value of the field synergy is relatively large at the corners, indicating that large flow resistance appears there. From the perspective of drag reduction, the flow near these corners should be optimized, namely, the speed distributor should be added there, which is consistent with the result of Fig. 4.

Indeed, compared to the original flow field, the flow resistance is significantly reduced in the optimized flow field after adding the speed distributor.

It can be used as a general guide for finding the target location for optimization according to the place where the cosine of the field synergy angle in the actual flow field is greater than 0.7.

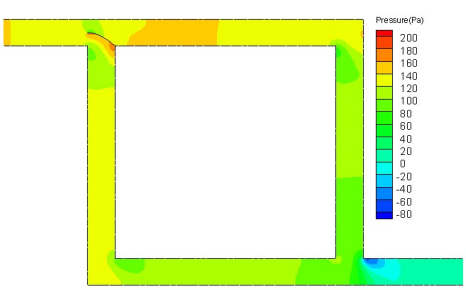

(a) pressure distribution

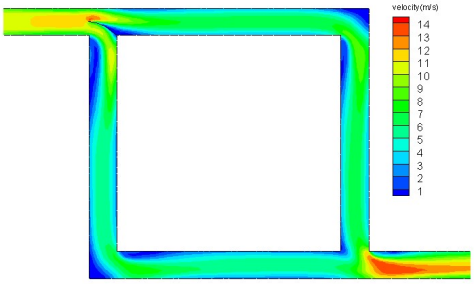

(b) velocity distribution

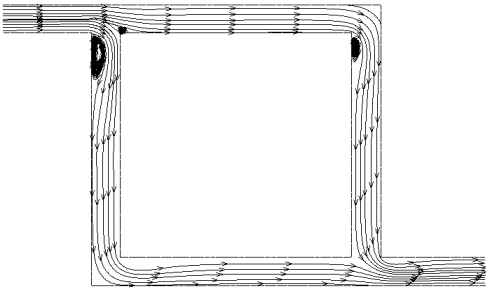

(c) streamline distribution

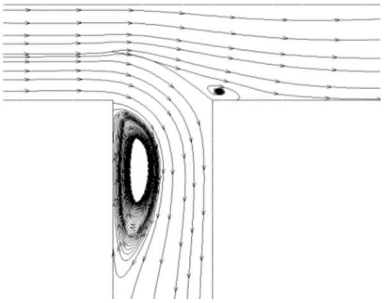

(d) local streamline distribution

Fig. 5. Optimized flow in the parallel conduit after adding the speed distributor.

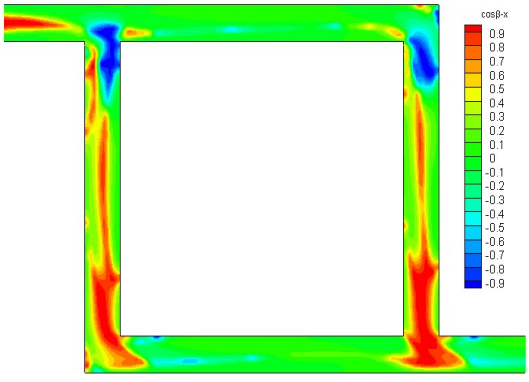

(a) Cosine-value in the x direction.

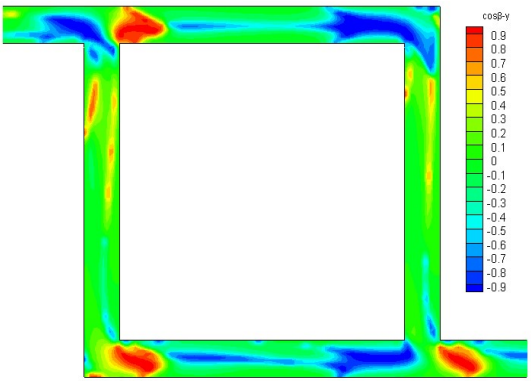

(b) Cosine-value in the y direction.

Fig. 6. Cosine value distribution of the synergy angle in the original parallel flow.

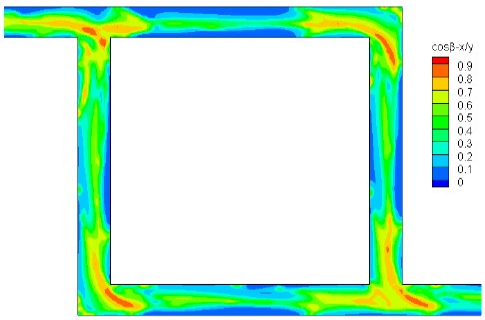

(a) The square mean of the cosine value of the field synergy angle.

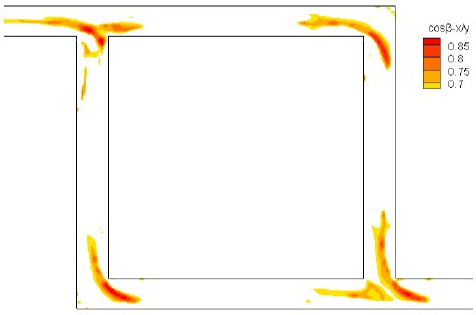

(b) The square mean of the cosine with the value larger than >0.7.

Fig. 7. Contour of the cosine squared average in the optimized parallel flow field.

Table 1 Comparison between numerical results and experimental data

Working Condition	Parameter	Simulation results	Monitored data	Error
50% load	Cold primary air pressure (kPa)	9.813	9.800	0.134%
	Pressure difference between inlet and outlet (Pa)	1760.351	----	----
	Air preheater pressure difference (Pa)	660.680	640.036	3.225%
	Hot air temperature ($^{\circ}C$)	293.154	292.055	0.376%
	Average temperature at the exit ($^{\circ}C$)	194.956	199.500	-2.278%
100% load	Pressure difference between inlet and outlet (Pa)	2546.462	----	----
	Air preheater pressure difference (Pa)	1491.600	1427.739	4.473%
	Hot air temperature ($^{\circ}C$)	316.523	313.572	0.941%
	Average temperature at the exit ($^{\circ}C$)	196.588	199.500	-1.460%

4. NUMERICAL APPLICATIONS

For a general flow, the first step is to find the target location for optimization according to the place where the cosine of the field synergy angle in the actual flow field is greater than 0.7. Secondly, the starting and ending points of the baffle are determined based on the streamline differences between the ideal flow field and the original actual flow field. Thirdly, the shape of the baffle should be designed with reference to the streamline of the ideal flow field to make the optimized flow field as close as possible to the ideal flow field after adding the baffle. Finally, comparing the flow field before and after optimization to evaluate the performance. If the performance is satisfactory, the dimensions of the deflector can be determined, and even optimized for the next loop.

4.1 Numerical optimization of a multi-pipe system

The primary air duct system in thermal power plant is composed of multiple pipelines and belongs to a multi-pipe combination system with relatively simple internal structure, as shown in Fig. 8. It includes a cold primary air duct flow and a hot primary air duct flow, and an air preheater for heating the primary air. To reduce the flow resistance and save energy for the power plant, the flow field in the primary air duct system of a boiler will be simulated and optimized by using the above field synergy principle for turbulent flow and minimum mechanical energy dissipation principle in this section.

4.1.1 Numerical simulation and validation

The geometric model was unstructured meshed using the ANSYS ICEM, and 3 boundary layer meshes were added to the walls to improve the calculation accuracy. Under the condition that the mesh quality and calculation accuracy are ensured and the calculation time is reasonable, the maximum mesh size is set to 0.3m, the number of meshes of the model is 2.21 million, and the mesh quality is above 0.3201, which meets the calculation requirements.

The simulation is carried out using the ANSYS FLUENT software in which, standard k-ε model with SIMPLEC algorithm and upwind-differencing scheme is utilized to solve the incompressible Reynolds mean equation.

Firstly, the original flow field in the primary air duct system is numerical simulated with the standard k-ε model under 50% and 100% load conditions, respectively. The numerical results are compared with the monitored data to validate the model, as summarized in Table 1. It is interesting to find that the flow field in the system can be well captured. The maximum numerical error is less than 5%, which lays a solid foundation for further analysis and optimization.

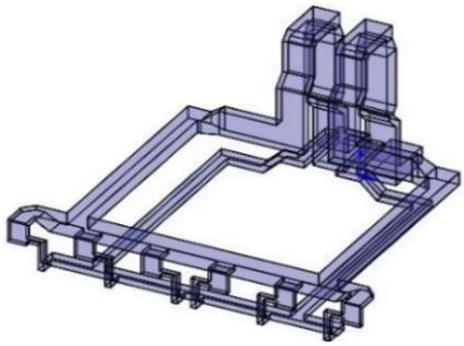

Fig. 8. Model of the primary air duct system in thermal power plant.

Additionally, it is found that the flow resistance in the primary air system comes mainly from the air preheater. For the 50% load condition, the pressure drop of the air preheater is 37.5% of the total pressure drop of the system, while for the 100% load condition, the pressure drop of the preheater increases to be 58.6% of the total pressure drop of the system. As the air preheater is fixed and could not be changed in the project, the drag reduction will come from the optimization of viscous resistance in other regions of the system.

4.1.2 Numerical optimization

To locate the internal structure of the system that needs to be optimized, field synergy analysis is performed on each pipe section to find the positions where the square mean of the cosine value of the field synergy angle is larger than 0.7. Three typical structures are shown in Fig. 9.

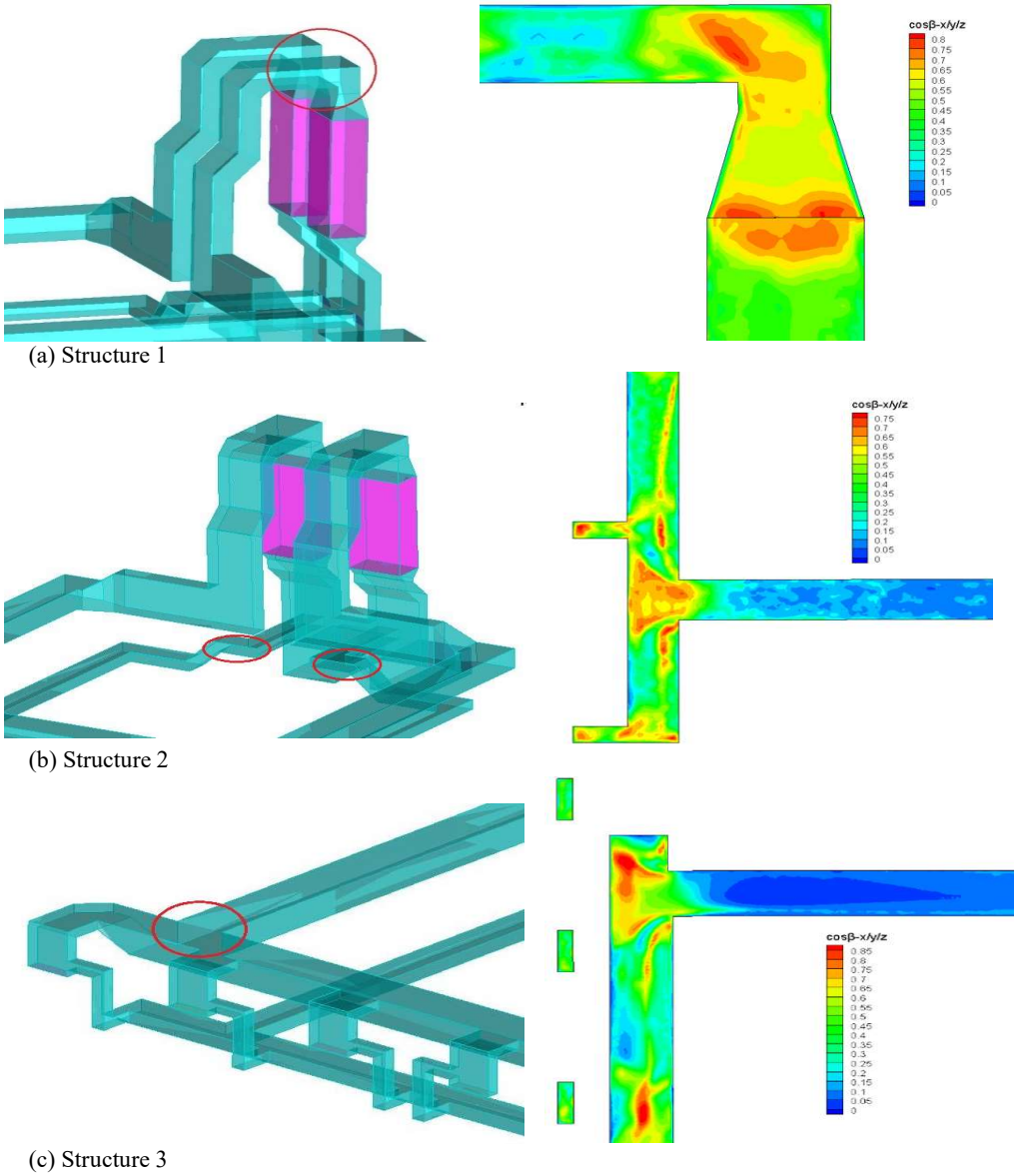

(a) Structure 1

(b) Structure 2

(c) Structure 3

Fig. 9. Three typical structures in the primary air duct system.

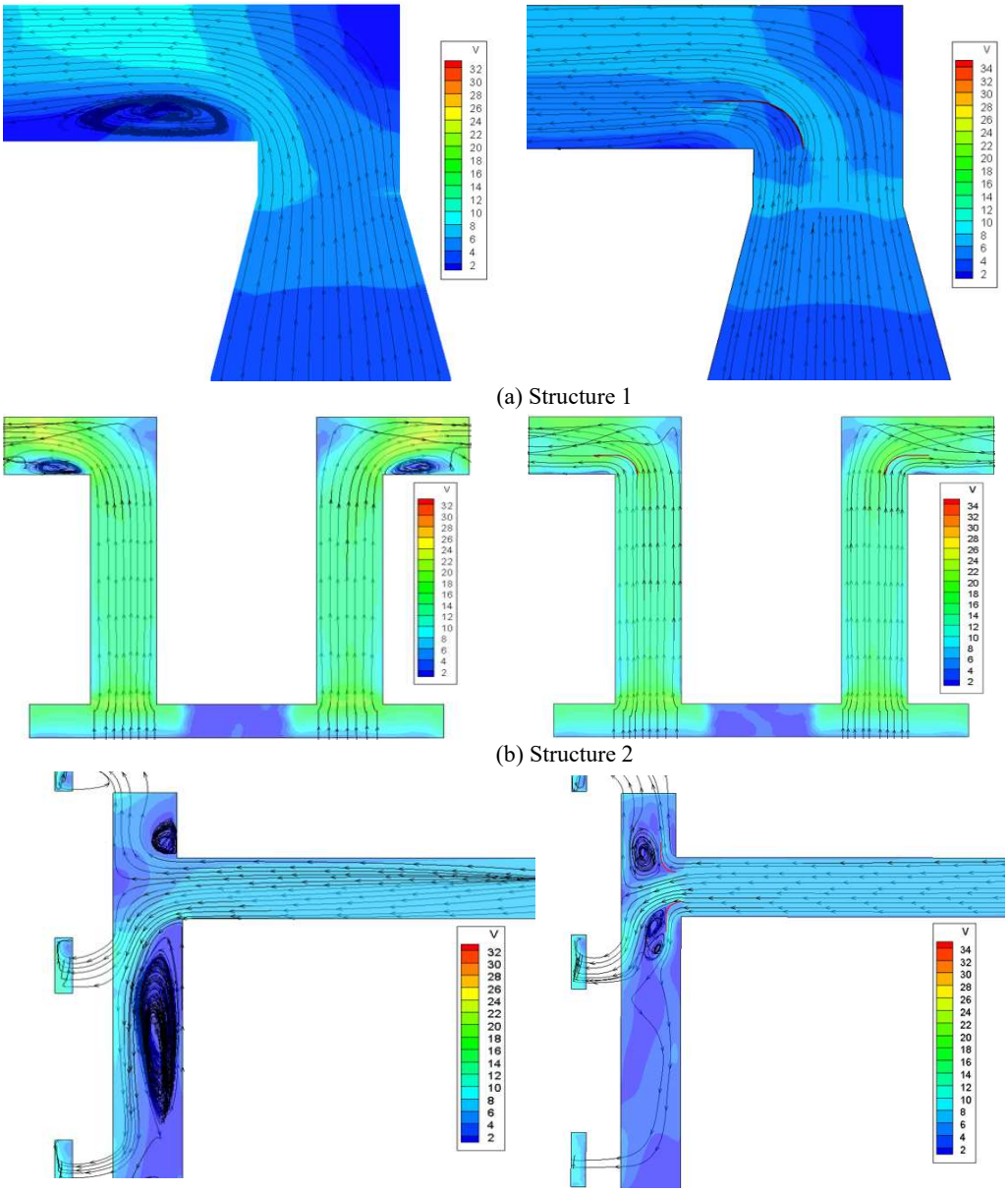

(a) Structure 1

(b) Structure 2

(c) Structure 3

Fig. 10. Velocity distribution before (left) and after (right) optimization.

It can be found that in each structure, the square mean of the cosine value of the field synergy angle is larger than 0.7 at the splitting point and the right-angle turning point, indicating that the flow resistance is large at these locations. At the same time, according to the streamline, the fluid velocity distribution is extremely non-uniform and the locations where the cosine value of the synergy angle is greater than 0.7 usually cause significant viscous dissipation. Therefore, it is necessary to optimize the structure here to reduce resistance.

Following the procedure presented in Section 3, the ideal flow field can be then obtained by solving the field synergy equations. Based on the ideal flow field, the speed splitter can be introduced to optimize the flow and reduce the resistance. The speed splitter acts as an interface that changes the flow by wall-fluid interactions, as shown in Fig. 10.

For Structure 1, it can be found that the vortex at the right-angled corner disappears almost completely after optimization, indicating that the speed splitter here breaks the vortex, changes the degree of synergy between the velocity field and the velocity gradient field, and contributes to reduce energy dissipation. As a result, the flow velocity distribution becomes more uniform. Similar effects can be observed for Structures 2 and 3.

For fluids, pressure is a measure of mechanical energy per unit volume. Quantitatively, the pressure drop before and after optimization for each structure is summarized in Table 2. The optimization for Structure 2 has the better effect, and the pressure drop decreases by about 40Pa, accounting for about

Table 2 Pressure drop before and after optimization

Local structure	Pressure drop before and after optimization (Pa)	Pressure drop reduction percentage (%)
Structure 1	19.98	1.31
Structure 2	41.15	2.69
Structure 3	22.67	1.48

Table 3 Comparison of the overall system before and after optimization

Working condition	50% load	100% load
Total pressure drop before optimization (Pa)	1760.35	2546.46
Total pressure drop after optimization (Pa)	1640.08	2229.28
Pressure drop difference (Pa)	120.28	178.88
Optimization percentage (%)	6.74	7.02
Optimization percentage (%) (removal of air preheater pressure drop)	10.94	16.96

2.7% of the total pressure drop. Although this number is small considering the pressure drop of the air preheater, it will increase to 8.4% if the pressure drop of the air preheater is not included. In the actual project, the air preheater is fixed and this effect is considerable. To evaluate the overall effect of the above optimizations, the primary air duct system with added speed splitters is numerical simulated under the actual working conditions of 50% load and 100% load respectively, and the statistics are summarized in Table 3.

For the original actual flow field, the computation error of the simulation of the original structure is less than 5% compared with the actual measured experimental data.

As mentioned above, the pressure drop formed by the internal resistance of the air preheater is about 40%-70%. Since in the actual project, the geometry of the air preheater cannot be obtained and changed, it is impossible to optimize the air preheater. Compared with the original primary air duct system, the optimization effect of the total pressure drop reaches 6.74% and 7.02% respectively. If the air preheater is not considered, the optimization effect of pressure drop changes to be 10.94%, 16.96% respectively under 50% and 100% load conditions. The effect is quite attractive in terms of saving energy.

4.2 Numerical optimization of a desulfurization tower outlet

Desulfurization tower has been widely used for pollutant control in power plant. As the outlet of the desulfurization tower is followed by a dust collector, there is a requirement for the flow field uniformity of the flue section to improve the performance of the system. In order to reflect the uniformity of the flow field, the flow field uniformity index γ is defined as (Tao *et al.* 2010):

$$\gamma = 1 - \frac{\sum_{i=1}^{n}\left[\left(\left|\phi_i - \bar{\phi}\right|\right)\right]A_i}{2\left|\bar{\phi}\right|\sum_{i=1}^{n}A_i} \tag{31}$$

Where $\bar{\phi} = \sum_{i=1}^{n}\phi_i A_i \Big/ \sum_{i=1}^{n} A_i$ is the field-averaged variable, i represents the surface mesh index with n mesh faces, and A_i represents the area of the local mesh. In this work, ϕ is the value of velocity in the flow field. From the definition, it can be deduced that the larger the γ value, the better the flow field uniformity.

Numerical simulation of a desulfurization tower outlet with the original geometric model is performed and the velocity distribution is shown in Fig. 10. It shows that when the flue gas flows out of the desulfurization tower, it is bounded by the wall, and the flow direction changes 90°. Under the effect of inertia, most of the flue gas rushes to the upper part, resulting in a large-scale high-speed region there and a low-speed region at the bottom, which is likely to cause backflow and increase the flow resistance. Obviously, this kind of flow field is not uniform enough and needs to be optimized.

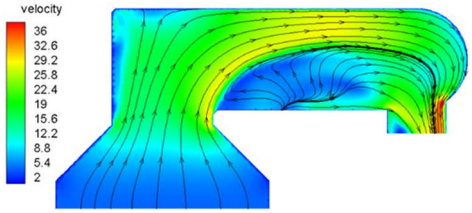

(a) the outlet of the desulfurization tower

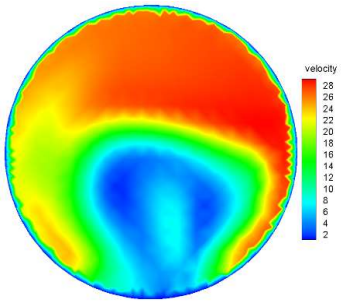

(b) cross section

Fig. 11. Velocity distribution at the outlet (case0).

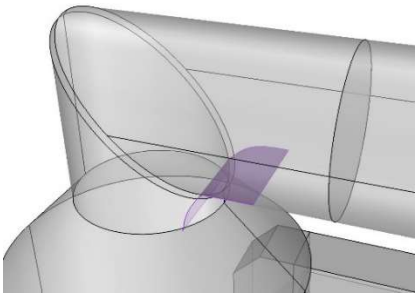

(a) The position of the first deflector (case1)

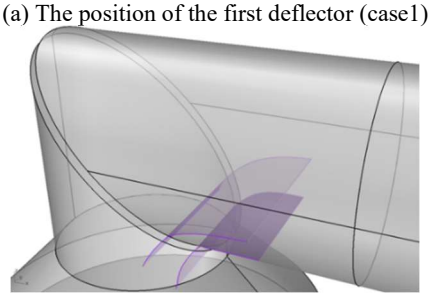

(b) The position of the second deflector (case2)

Fig. 12. Position of the deflectors.

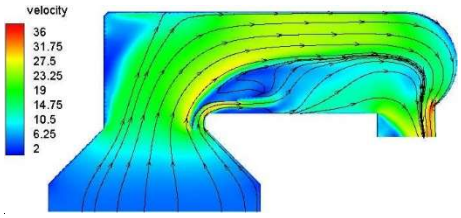

(a) the outlet of the desulfurization tower

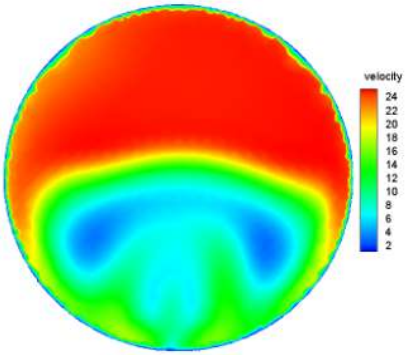

(b) cross section

Fig. 13. Velocity distribution at the outlet after the first optimization (case1).

The field synergy equations are firstly solved to get the ideal "complete cooperative" flow field. Based on the ideal flow field, a deflector is then added as an internal interface to optimize the original flow field (Fig. 12(a)). Under this geometric model, the flow is simulated and the results are presented in Fig. 13. The backflow is depressed and the velocity distribution at the bottom region becomes relatively uniform due to the addition of the deflector. However, the velocity distribution is still not so uniform in the middle region and the uniformity index of the cross section is just 68.71%, which needs further optimization.

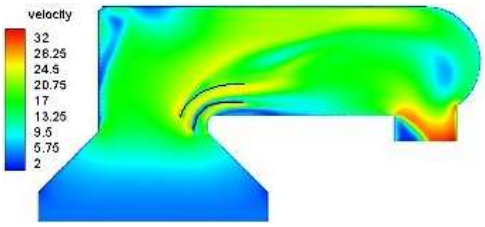

(a) the outlet of the desulfurization tower

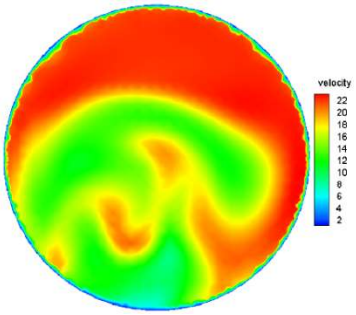

(b) cross section

Fig. 14. Velocity distribution at the outlet after second optimization (case2).

According to the velocity distribution in Fig.13, another deflector is added to further optimize the flow field, as shown in Fig.12(b). Numerical simulation of fluid flow in this new geometric model is conducted and the results are shown in Fig.14. The first deflector weakens or even eliminates the vortex structure at the bottom which depresses the backflow of the flue gas and reduces the flow resistance, and the newly added deflector further split a large amount of high-speed flue gas originally distributed in the upper region so that the distribution of flue gas on the entire section is more uniform.

To quantitatively assess the effect of the first and second optimization, the cross-sectional uniformity index for the cases without the deflector, with the addition of the first deflector, with the addition of the two deflectors is calculated and shown in Fig. 15. The corresponding pressure drop is also displayed. The uniformity of the flow field increases from the original 56% to 66% for the first optimization and 81% for the second optimization, and the pressure drop decreases from the original 487.5Pa to 375Pa for the first optimization and 337.5Pa for the second optimization. After adding two deflectors, the velocity distribution becomes quite uniform which meets the requirements of the project. This indicates that the field synergy method can be iteratively used for flow field optimization until satisfactory effect is achieved. Furthermore, the velocity distribution in Fig.14 shows a small range of stagnation zone of flow and it has potential to be further improved.

5. CONCLUSIONS

In this study, the principle of field synergy is firstly extended from laminar flow to turbulent flow. Compared with laminar flow, the flow resistance in

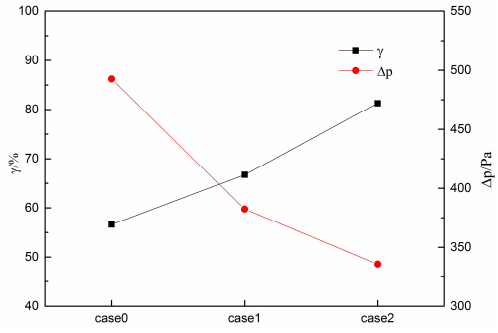

Fig. 15. Velocity uniformity index and pressure drop for different cases.

turbulent flow is not only related to the field synergy number, but also has relationship with the effective viscosity coefficient. Based on the irreversibility of dissipation in the flow process and the principle of minimum mechanical energy dissipation, the field synergy equations are derived and a general theoretical approach for flow field optimization is then developed. This approach is implemented and validated in a turbulent parallel flow conduit, and finally applied to industrial pipe flows. It demonstrates that the present approach is able to optimize flow field for different purposes by adding speed splitter or deflector as an interface at proper locations to change the interactions between fluid and walls. This approach is robust and easy to implement, providing a general tool for flow optimization.

REFERENCES

Addy, A. L., M. J. Morris and J. C. Dutton (1985). An investigation of compressible flow characteristics of butterfly valves. *Journal of Fluids Engineering* 107(4), 512.

Chen, Q., J. Ren and J. A. Meng (2007). Field synergy equation for turbulent heat transfer and its application. *International Journal of Heat and Mass Transfer* 50(25-26), 5334-5339.

Chen, Q., J. Ren and Z. Guo (2008). Fluid flow field synergy principle and its application to drag reduction. *Chinese Science Bulletin* 53(11), 1768-1772.

Dutta, P., S. K. Saha, N. Nandi and N. Pal (2016). Numerical study on flow separation in 90° pipe bend under high Reynolds number by k-ε modelling. *Engineering Science and Technology, an International Journal* 19(2), 904-910.

Guo, Z. Y., D. Y. Li and B. X. Wang (1998). A novel concept for convective heat transfer enhancement. *International Journal of Heat and Mass Transfer* 41(14), 2221-2225.

Hu, X. P., Y. X. Hong and X. H. Deng (2012). Numerical Simulation of Laminar Heat Transfer Enhancement in Tube Side. *Guangzhou Chemical Industry* 40(03), 36-39.

Hui, W. (2014, February). *Numerical simulation of turbulent flow behind a butterfly valve placed in a dual-elbow channel and its experimental analysis.* Master thesis, Shanghai Jiao Tong University, Shanghai, China.

Jia, X. H., X. H. Peng and X. S. Long (2011). Numerical Simulation and Optimization of Flow Field in Elbow Pipes with Baffle. *Journal of Southwest University (Natural Science Edition)* 33(3), 139-143.

Khanorkar, P. M. and R. E. Thombre (2013). CFD analysis of natural convection flow through vertical pipe. *Int. J. Mech. Eng. & Rob. Res* 2, 371-378.

Kim, J., M. Yadav and S. Kim (2014). Characteristics of secondary flow induced by 90-degree elbow in turbulent pipe flow. *Engineering Applications of Computational Fluid Mechanics* 8(2), 229-239.

Lu, G. (2014, May). *The Study on the Turbulent Field Synergy model and its Application to Drag Reduction*. Master thesis, Dalian University of Technology, Liaoning, China.

Lv, J. S. (2014, September). *Fundamental Study on the Fluid Flow Analysis Using Field Synergy Principle.* Ph. D. thesis, Dalian University of Technology, Liaoning, China.

Marjavaara, B. D. and T. S. Lundström (2006). Redesign of a sharp heel draft tube by a validated CFD - optimization. *International journal for numerical methods in fluids* 50(8), 911-924.

Okafor, C. V., O. R. Ononye and A. U. Okeke (2020). Analysis of Water Flow in Tee-junction Pipes Using CFD. *Journal of Multidisciplinary Engineering Science and Technology (JMEST)* 7(3),11550-11553.

Rao, Y., K. Chang, S. Wang, L. I. Jianmin and M. Yang (2016) Numerical simulation of fluid flow characteristic in 90° bend pipe. *Journal of Changzhou University* (Natural Science Edition) 28(3),65-69.

Rao, A. (2018). *Cfd simulation of fluid flow through T, Y and y-junction of pipes*. LAMBERT Academic Publishing.

Rodriguez, S. (2019). *Applied computational fluid dynamics and turbulence modeling.* Springer International Publishing.

Tao, W. Q. (2001). *Numerical heat transfer* (the Second Edition). Xi'an: Xi'an Jiaotong University Press, China.

Tao, H., H. Chen, J. Xie, Z. Shu, Y. Hu and H. Lu (2010). Flow uniformity index based on area-weighted and mass-weighted average velocity. *CIESC Journal S* 2,116-120.

Tao, W. Q., Y. L. He and L. Chen (2019). A comprehensive review and comparison on heatline concept and field synergy

principle. *International Journal of Heat and Mass Transfer* 135, 436-459.

Wu, G. (2013, May). *Numerical Simulation for dynamic characteristics of axial flow check.* Master thesis, Lanzhou University of Technology, Gansu, China.

Yang, G., G. Wu, X. Liu, W. Cao and M. Xu (2013). Dynamic characteristics of axial flow check valve. *Journal of Drainage and Irrigation Machinery Engineering/ Paiguan Jixie Gongcheng Xuebao* 31(1), 46-49.

Yue, Z. H. A. O. (2011, March). *Numerical Simulation on Local Resistance Based on CFD.* Master Thesis, Northeast Petroleum University, Heilongjiang, China.

Zhang, B., J. Lv and J. Zuo (2014). Compressible fluid flow field synergy principle and its application to drag reduction in variable-cross-section pipeline. *International Journal of Heat and Mass Transfer* 77, 1095-1101.

Zhao, H., M. Ma and X. Su (2015). Internal flow field simulation and design optimization based on CFD pipeline pig structure. *Oil & Gas Storage and Transportation* 05,562-566.

Zuo, J. (2012, May). *Study on The Optimal Design of The Vapour Ejector with Field Synergy Principle*. Master thesis, Dalian University of Technology, Liaoning, China